Modulated Predictive Current Control Technique for a Three-Phase Four-Wire Active Power Filter based on H-bridge Two-Level Converter

Alfredo Renault, Jorge Rodas, Leonardo Comparatore, Julio Pacher and Raul Gregor
Laboratory of Power and Control Systems, Facultad de Ingeniería, Universidad Nacional de Asunción, Paraguay
E-mail: {arenault, jrodas, lcomparatore, jpacher & rgregor}@ing.una.py

***Abstract*—Finite-control-set model-based predictive current control (FCS-MPCC) technique is distinguished by a variable switching frequency which causes high harmonic distortion a low sampling frequency. This latter could be considered an undesired behavior for active power filter for grid-connected applications. To overcome this issue, this paper proposes a modulated FCS-MPCC applied to a three-phase four-wire active power filter based on H-bridge converter. Simulation results are developed to demonstrate the efficiency of the proposed modulated FCS-MPCC comparing with classic FCS-MPCC, thus concluding the advantages and limitations of each technique at transient and steady states.**

***Index Terms*—Active power filter, current control, H-bridge converter, model predictive control.**

NOMENCLATURE

APF	Active power filter.
CHB	Cascade H-bridge.
FCS-MPCC	Finite-control-set MPCC.
MPCC	Model-based predictive current control.
PCC	Point of common coupling.
STATCOM	Static compensator.
THD	Total harmonic distortion.
C_{dc}	dc-link capacitor.
g_a, g_b, g_c, g_n	FCS-MPCC cost functions.
i_s^a, i_s^b, i_s^c, i_s^n	Power grid phase currents.
v_s^a, v_s^b, v_s^c	Power grid phase voltage.
i_L^a, i_L^b, i_L^c, i_L^n	Load phase currents.
i_c^a, i_c^b, i_c^c, i_c^n	STATCOM phase currents.
$\hat{i}_c^a$, $\hat{i}_c^b$, $\hat{i}_c^c$, $\hat{i}_c^n$	STATCOM phase current predictions.
$i_{c\alpha}$, $i_{c\beta}$, i_{c0}	STATCOM currents in the $\alpha-\beta-0$ subspace.
i_c^{a*}, i_c^{b*}, i_c^{c*}, i_c^{n*}	STATCOM current references.
v_c^a, v_c^b, v_c^c	STATCOM phase voltages.
n_c	Number of cells.
P_c^*	Instantaneous active power reference.
P_0	Instantaneous active power 0 sequence.
Q_c^*	Instantaneous reactive power reference.
Q_L	Instantaneous reactive load power.
$\mathbf{T}$	Clarke's transformation matrix.

I. INTRODUCTION

APFs based on H-bridge converters equipped with SiC-MOSFETs switching devices have several advantages such as the possibility of scalability, modular structure and high switching frequency [1], [2]. Due to these advantages, SiC-MOSFETs H-bridge converters have attracted the attention of the research community and currently, they are considered as a real competitive topology in the new generation APF for grid-connected converters [3], [4].

Nowadays, FCS-MPCC is applied with success in complex power electronic applications such as APFs [5], multiphase machines [6], matrix converters [7], among others. The easy inclusion of non-linearities and constraints, as well as its fast dynamic response, makes FCS-MPCC an alternative to classic control methods. Moreover, thanks to the improvement of the microprocessor technology, the implementation of FCS-MPCC algorithm could be performed at higher sampling frequency [8], [9]. However, one of the main disadvantage presented by FCS-MPCC is its variable switching frequency produced by the optimal voltage vectors. This issue may produce current ripple with high peaks in the current to the converter output and power losses [10], [11].

In this context, this article proposes a modulated FCS-MPCC method applied to a four-wire three-phase APF based on two-level H-bridge converters operated at fixed switching frequency through a switching pattern [12], [13]. This allows a better distribution of switching in the power semiconductor devices, thus reducing power losses and the current ripple in the output current of the converter and reducing the THD injected into the electrical power grid [14], [15]. To check the feasibility of the proposal, a comparison is made with the classic FCS-MPCC and the modulated FCS-MPCC, simulation results are presented using the MATLAB/Simulink tool. This paper is organized as follows: Section II describes the three-phase four-wire CHB STATCOM topology. In the same section, the classic FCS-MPC is also introduced. Then, Section III exposes the proposed modulated FCS-MPCC strategy. Section IV illustrates the performance of the proposed techniques considering the simulation results. Finally, the conclusion is presented in Section V.

II. SYSTEM DESCRIPTION

The system under study is a three-phase four-wire APF based on CHB connected in parallel to the electric power grid as shown in Fig. 1. The APF consists of four independent

978-1-5386-2910-9/18/$31.00

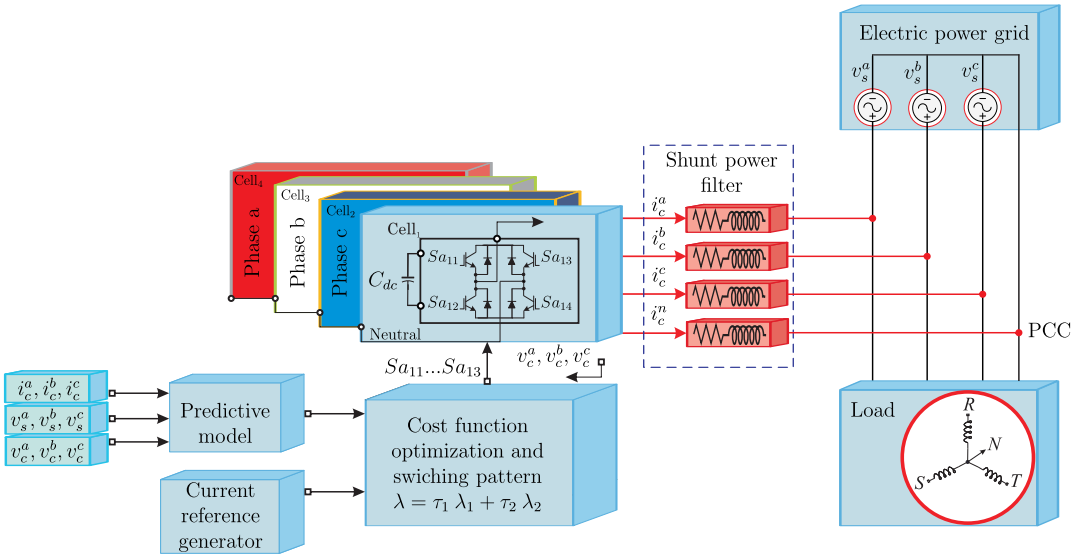

Fig. 1. The control scheme of the proposed modulated FCS-MPCC.

CHB cells with dc-link corresponding to the phases a, b, c and n [16], [17]. Each CHB cell contains four switching devices SiC-MOSFET (which can operate up 100 kHz) connected in H-bridge S_{fxy} to control each cell, being f the phase ($f = a$, b o c), x cell number in each phase and y the switching device in each cell ($y = 1$, 2, 3 or 4). Table I shows the permitted combinations of the activation signals of the switching devices and the voltage vectors at the output of the converter, for the case of phase a, for example. The analysis is similar for the other cells avoiding the short circuit in the dc-link. The dynamics of the system model is obtained using the Kirchhoff circuit laws. The unbalance of the three-phase voltages of the electrical power grid, as well as the capacitance and dc-link voltages, are beyond the scope of this document, and only the equilibrium conditions are considered to obtain the system model. The STATCOM based on the CHB converter is connected to the PCC. Then, applying the laws of Kirchhoff for the ac side of STATCOM, the following equations are obtained:

TABLE I
POSSIBLE COMBINATIONS OF ACTIVATION SIGNALS

Sa_{11}	Sa_{13}	Sa_{12}	Sa_{14}	v_c^a
1	0	0	1	$+v_{\mathrm{dc}}$
1	1	0	0	0
0	0	1	1	0
0	1	1	0	$-v_{\mathrm{dc}}$

$$\begin{aligned}
\frac{\mathrm{d}i_c^a}{\mathrm{d}t} &= 1/L_f\,(v_s^a - R_f\,i_c^a - n_c\,Sa_{xy}\,v_{\mathrm{dc}}^a)\\
\frac{\mathrm{d}i_c^b}{\mathrm{d}t} &= 1/L_f\,\left(v_s^b - R_f\,i_c^b - n_c\,Sb_{xy}\,v_{\mathrm{dc}}^b\right)\\
\frac{\mathrm{d}i_c^c}{\mathrm{d}t} &= 1/L_f\,(v_s^c - R_f\,i_c^c - n_c\,Sc_{xy}\,v_{\mathrm{dc}}^c)\\
\frac{\mathrm{d}i_c^n}{\mathrm{d}t} &= 1/L_f\,(v_s^n - R_f\,i_c^n - n_c\,Sc_{xy}\,v_{\mathrm{dc}}^n)
\end{aligned} \tag{1}$$

$$\begin{aligned}
\frac{\mathrm{d}v_{\mathrm{dc}}^a}{\mathrm{d}t} &= \frac{Sa_{xy}}{C_{\mathrm{dc}}}i_c^a - \frac{v_{\mathrm{dc}}^a}{R_{\mathrm{dc}}\,C_{\mathrm{dc}}}\\
\frac{\mathrm{d}v_{\mathrm{dc}}^b}{\mathrm{d}t} &= \frac{Sb_{xy}}{C_{\mathrm{dc}}}i_c^b - \frac{v_{\mathrm{dc}}^b}{R_{\mathrm{dc}}\,C_{\mathrm{dc}}}\\
\frac{\mathrm{d}v_{\mathrm{dc}}^c}{\mathrm{d}t} &= \frac{Sc_{xy}}{C_{\mathrm{dc}}}i_c^c - \frac{v_{\mathrm{dc}}^c}{R_{\mathrm{dc}}\,C_{\mathrm{dc}}}\\
\frac{\mathrm{d}v_{\mathrm{dc}}^n}{\mathrm{d}t} &= \frac{Sc_{xy}}{C_{\mathrm{dc}}}i_c^n - \frac{v_{\mathrm{dc}}^n}{R_{\mathrm{dc}}\,C_{\mathrm{dc}}}
\end{aligned} \tag{2}$$

being R_{dc} a resistor connected in parallel to C_{dc} that concentrates the overall losses in the dc side and R_f, L_f are the resistance and inductor, respectively, that work as a filter at the output of the CHB.

A. Classic FCS-MPCC strategy

Classic FCS-MPCC uses the mathematical model of the system, namely predictive model, to predict its future behavior. In this case, the differential equations of the system in the ac side is represented by the following equations:

$$\begin{aligned}
\frac{\mathrm{d}i_c^a}{\mathrm{d}t} &= 1/L_f\,(v_s^a - v_c^a - R_f\,i_c^a)\\
\frac{\mathrm{d}i_c^b}{\mathrm{d}t} &= 1/L_f\,\left(v_s^b - v_c^b - R_f\,i_c^b\right)\\
\frac{\mathrm{d}i_c^c}{\mathrm{d}t} &= 1/L_f\,(v_s^c - v_c^c - R_f\,i_c^c)\,.\\
\frac{\mathrm{d}i_c^n}{\mathrm{d}t} &= 1/L_f\,(v_s^n - v_c^n - R_f\,i_c^n)\,.
\end{aligned} \tag{3}$$

Then, the predictive model can be obtained by using a forward-Euler discretization method due to its simplicity. However other discretization methods can be used such as

the matrix factorization introduced by Cayley-Hamilton. The discrete-time model is given by [18], [19]:

$$\begin{aligned}
\hat{i}^a_{c[k+1|k]} &= A_1\, i^b_{c[k]} + T_s/L_f\, \left(v^a_{s[k]} - v^a_{c[k]}\right)\\
\hat{i}^b_{c[k+1|k]} &= A_1\, i^b_{c[k]} + T_s/L_f\, \left(v^b_{s[k]} - v^b_{c[k]}\right)\\
\hat{i}^c_{c[k+1|k]} &= A_1\, i^c_{c[k]} + T_s/L_f\, \left(v^c_{s[k]} - v^c_{c[k]}\right)\\
\hat{i}^n_{c[k+1|k]} &= A_1\, i^n_{c[k]} + T_s/L_f\, \left(v^n_{s[k]} - v^n_{c[k]}\right)
\end{aligned} \tag{4}$$

being $A_1 = \left(1 - \frac{R_f T_s}{L_f}\right)$.

In the case of a current control, the typical cost function is defined as the difference between reference currents and the predicted currents [20], [21]:

$$\begin{aligned}
g_a &= \| \, i_c^{a^*} - \hat{i}^a_{c[k+1]} \, \|^2\\
g_b &= \| \, i_c^{b^*} - \hat{i}^b_{c[k+1]} \, \|^2\\
g_c &= \| \, i_c^{c^*} - \hat{i}^c_{c[k+1]} \, \|^2\\
g_n &= \| \, i_c^{n^*} - \hat{i}^n_{c[k+1]} \, \|^2 .
\end{aligned} \tag{5}$$

Next, the cost function is evaluated for each switching states and for each phase. The switching state that minimizes the cost function is applied to each phase of the CHB STATCOM during the next sampling time causing a variable switching frequency for each phase.

B. Current reference generation

For the evaluation of the cost function in (5) is necessary the current references. For simplicity, the phase currents and voltages are translated to the $\alpha - \beta - 0$ subspace by using Clarke's transformation matrix:

$$\mathbf{T} = \sqrt{\frac{2}{3}} \begin{bmatrix} 1 & -\frac{1}{2} & -\frac{1}{2} \\ 0 & \frac{\sqrt{3}}{2} & -\frac{\sqrt{3}}{2} \\ \frac{1}{\sqrt{2}} & \frac{1}{\sqrt{2}} & \frac{1}{\sqrt{2}} \end{bmatrix}. \tag{6}$$

Then, the current references in $\alpha-\beta-0$ subspace in function of active and reactive power are:

$$\begin{bmatrix} i^*_{c\alpha} \\ i^*_{c\beta} \end{bmatrix} = \frac{1}{(v_{s\alpha})^2 + (v_{s\beta})^2} \begin{bmatrix} v_{s\alpha} & v_{s\beta} \\ v_{s\beta} & -v_{s\alpha} \end{bmatrix} \begin{bmatrix} P^*_c \\ Q^*_c \end{bmatrix}. \tag{7}$$

and i^*_{c0} simplified is:

$$i^*_{c0} = i_{L0} \tag{8}$$

Then the STATCOM does compensate the alternate part of the active power and the instantaneous reactive power reference can be written as [22], [23]:

$$P^*_c = -\tilde{P}_L \tag{9}$$

$$Q^*_c = -Q_L = v_{s\alpha}\, i_{L\beta} - v_{s\beta}\, i_{L\alpha} \tag{10}$$

$$P^*_{c0} = -P_{L0} = -i_{L0} v_{s0} \tag{11}$$

where Q_L and P_{L0} are compensated by the CHB STATCOM system. The STATCOM phase currents references used in the optimization process are:

$$\begin{bmatrix} i_c^{a^*} \\ i_c^{b^*} \\ i_c^{c^*} \end{bmatrix} = \mathbf{T}^{-1} \begin{bmatrix} i^*_{c\alpha} \\ i^*_{c\beta} \\ i^*_{c0} \end{bmatrix}. \tag{12}$$

III. Proposed modulated FCS-MPCC strategy

This predictive control strategy uses two active vectors in conjunction with a switching pattern Fig. 2, therefore it can be seen as space vector modulation. This method first follows the same procedure as classic FCS-MPCC strategy explained in the previous section. After the evaluation of the current predictions (4), currents references (12) and cost function (5), the optimum voltage vector is located in sector given by the two active vector nearest to the optimum switching state. Then, the proposed method evaluates the cost function, namely λ_1 and λ_2, of each active voltage vectors. Next, the duty cycles are computed by solving the following equation:

$$\overbrace{K/\lambda_1}^{\tau_1} + \overbrace{K/\lambda_2}^{\tau_2} = T_s. \tag{13}$$

By solving (13) it is possible to obtain the expression for K and the expressions for the duty cycles for each vector, that are given as:

$$\begin{aligned}
\tau_1 &= \frac{\lambda_2}{\lambda_1 + \lambda_2}\\
\tau_2 &= \frac{\lambda_1}{\lambda_1 + \lambda_2}.
\end{aligned} \tag{14}$$

Then, according to these expressions, the new cost function, which is evaluated at every sampling time for each phase, is defined as:

$$\lambda = \tau_1\, \lambda_1 + \tau_2\, \lambda_2. \tag{15}$$

Finally, the optimization algorithm selects the optimum vector S_f^{opt} for each firing signals of each cell by the evaluation and minimization of the predefined cost function represented by (15). To make the thing clearer, Algorithm 1 summarizes the optimization process.

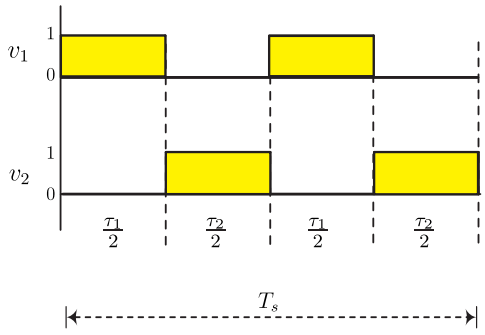

Fig. 2. Switching pattern of the proposed modulated FCS-MPCC.

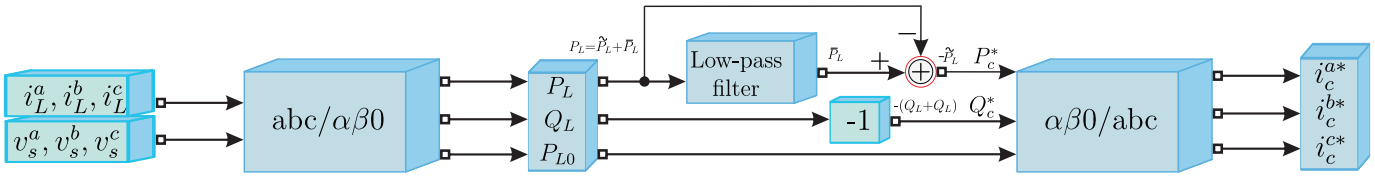

Fig. 3. Current reference generation for the FCS-MPCC.

Algorithm 1 Optimization algorithm of the proposed current controller

1. Initialize $g_o^a := \infty, g_o^b := \infty, g_o^c := \infty, g_o^n := \infty, \eta := 0$
2. Compute the STATCOM current references (7).
3. **while** $\eta \leq \varepsilon$ **do**
4. $\quad S_{f_{ij}} \leftarrow S_{f_{ij}}^{\eta} \ \forall\ i\ \&\ j = 1,\ 2,\ 3$
5. $\quad$ Compute the STATCOM prediction currents (4).
6. $\quad$ Compute the cost function, (5).
7. $\quad$ **if** $g^a < g_o^a$ **then** $\quad g_o^a \leftarrow g^a, \quad S_a^{opt} \leftarrow S_{a_{ij}}$
8. $\quad$ **end if**
9. $\quad$ **if** $g^b < g_o^b$ **then** $\quad g_o^b \leftarrow g^b, \quad S_b^{opt} \leftarrow S_{b_{ij}}$
10. $\quad$ **end if**
11. $\quad$ **if** $g^c < g_o^c$ **then** $\quad g_o^c \leftarrow g^c, \quad S_c^{opt} \leftarrow S_{c_{ij}}$
12. $\quad$ **end if**
13. $\quad$ **if** $g^n < g_o^n$ **then** $\quad g_o^n \leftarrow g^n, \quad S_n^{opt} \leftarrow S_{n_{ij}}$
14. $\quad$ **end if**
15. $\quad \eta := \eta + 1$
16. **end while**
17. Compute the new cost function and duty cycles (13)-(15).
18. Applied optimal switching states following the switching pattern, Fig. 2.

IV. Simulation Results

This section theoretically verifies the performance of the proposed modulated FCS-MPCC by using MATLAB/Simulink simulation tool. A numerical integration based on Ode1 Euler was used for the calculation of step by step variables in the time domain with a relative tolerance of 1e-6. The electrical parameters, as well as the FCS-MPCC parameters using for the simulations, are shown in Table II. The system is first operated with balanced load (from $t = 0$ s to $t = 0.04$ s) when suddenly the load changes from $R_L = 23.2\ \Omega$ to $R_L = 46.4\ \Omega$ in phase "a". Note that the two-level CHB STATCOM is connected at $t = 0.1$ s.

Fig. 4(a) and Fig. 4(b) show the active and reactive compensation (above figure), the APF output current (middle figure) and the output voltage of the CHB STATCOM (lower figure), for classic FCS-MPCC and the proposed modulated FCS-MPCC, respectively. It can be noticed that both controllers show a fast dynamic response and good reactive power compensation in the power grid $Q_s = 3\,000$ VAR to a mean value to zero. However, the classic FCS-MPCC shows a higher ripple in the current injected to the grid i_c^a as well as in the reactive power. Moreover, the proposed FCS-MPCC gives better current tracking and a fixed switching pattern of the output voltage of the CHB STATCOM.

TABLE II
Parameters Description

PARAMETER	two-level CHB STATCOM SIMBOLS	VALUE	UNIT
Electric frequency on the power grid	f_e	50	Hz
Voltage of electric power grid	v_s	310.2	V
Filter resistance	R_f	0.09	Ω
Filter inductance	L_f	3	mH
dc-link voltage	v_{dc}	342	V
	Load parameters		
Load resistance	R_L	23.2	Ω
Neutral load resistance	R_{Ln}	1	Ω
Change Load	R_L	46.4	Ω
Load inductance	L_L	55	mH
	Predictive control parameters		
Sampling frequency	f_s	40	kHz
Sampling time	T_s	25	μs
Active power reference	P_c^*	$-\tilde{P}_L$	W
Reactive power reference	Q_c^*	$-Q_L$	VAr
Zero sequence instantaneous power	P_{c0}^*	$-P_{L0}$	W

Considering the THD as a parameter of performance, the proposed controller gives a THD=3.64% while the classic FCS-MPCC gives 16.78% as shown in Fig. 5 (bottom). This improvement meets the grid-connected codes related to the limits of the low-order harmonics that can be injected into the power grid. An improvement in the grid current is also introduced by the proposed controller, as can be seen in Fig. 5 (above).

Finally, Fig. 6 shows the neutral current elimination of the proposed modulated FCS-MPCC, a neutral current compensation of 4.5 A peak to peak can be observed at a mean value of zero in the power grid.

V. Conclusion

In this paper, a modulated FCS-MPCC is proposed in order to provide a constant switching frequency of the power switching devices (i.e. SiC-MOSFETs). This strategy is applied as a current regulator of a two-level three-phase four-wire CHB STATCOM. As observed from results, the proposed controller provides also a fast dynamic response and easy inclusion of constraints as classic FCS-MPCC, compensating the reactive power and eliminating the neutral current. Nonetheless, the proposed controller also provides a reduction of the current ripples as well as a reduction of the THD (around 13.14 %), compared with the classic FCS-MPCC.

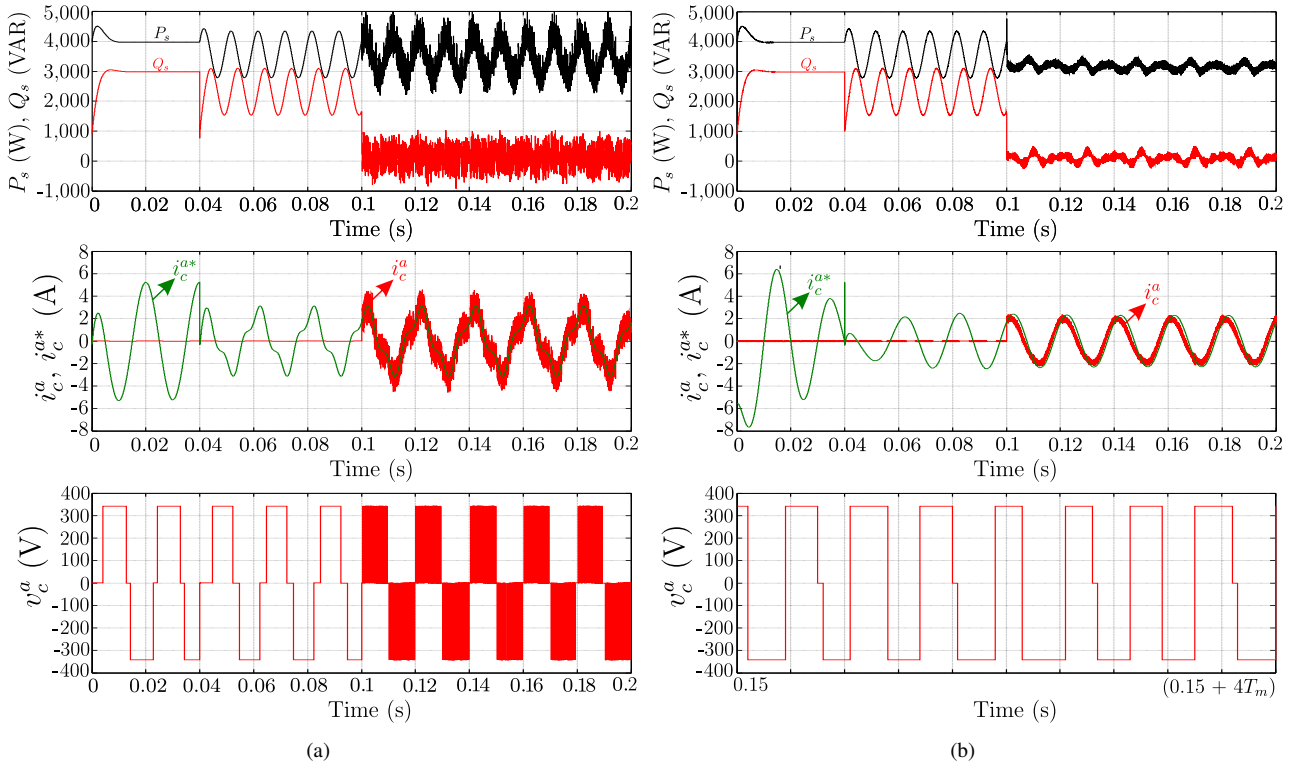

(a) (b)

Fig. 4. Comparison of each controller considering: (above) the active power and reactive power compensation, (middle) current of CHB STATCOM and current reference, (bottom) output voltage of CHB STATCOM. (a) Classic FCS-MPCC, (b) Proposed modulated FCS-MPCC.

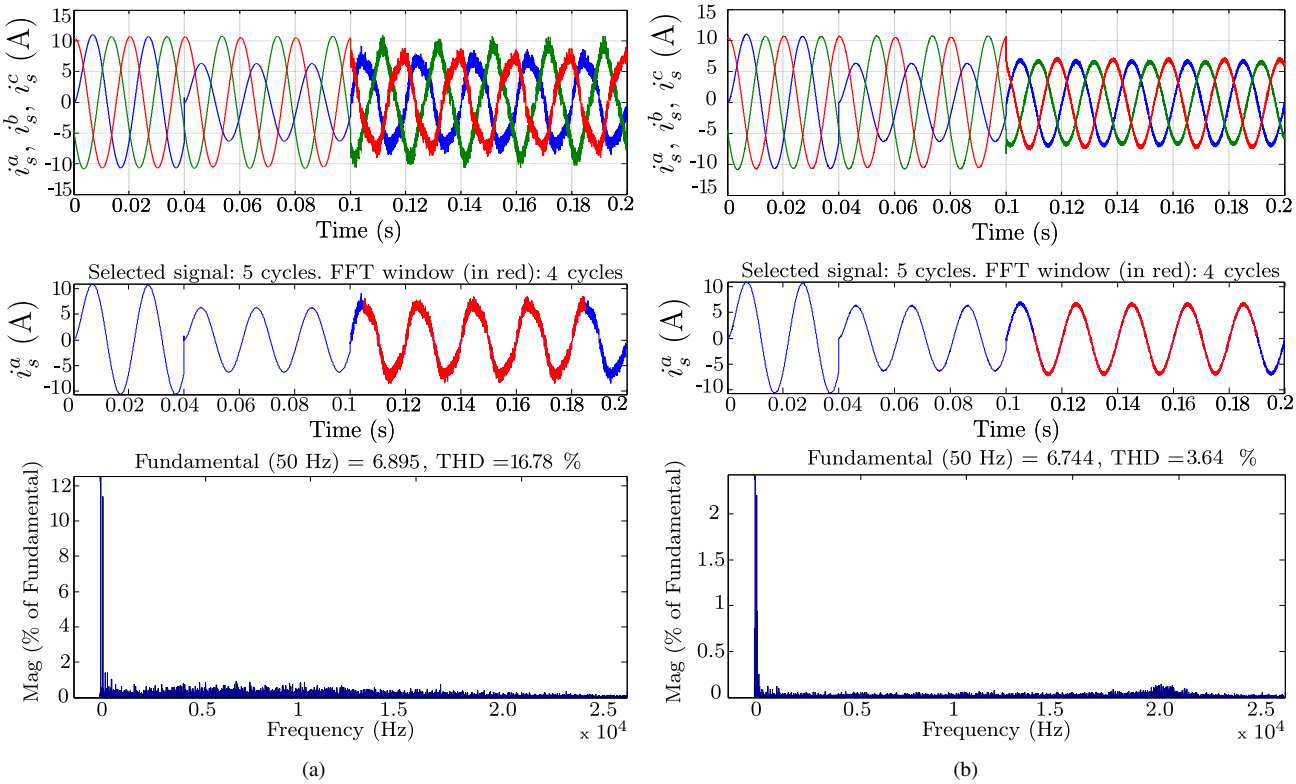

(a) (b)

Fig. 5. Comparison of each controller considering: (above) the power grid current evolution, (middle) four sample cycles of power grid current in phase "a" for the calculation of THD, (bottom) the THD of power grid current. (a) Classic FCS-MPCC, (b) Proposed modulated FCS-MPCC.

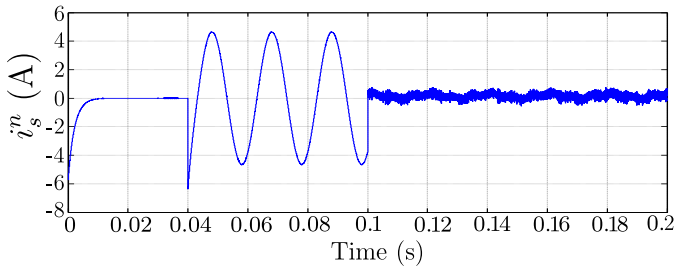

Fig. 6. Neutral current elimination of the modulated FCS-MPCC.

ACKNOWLEDGMENT

The authors wish to thank the financial support from the Paraguayan Science and Technology National Council (CONACYT) through project 14-INV-096.

REFERENCES

[1] J. Pacher, J. Rodas, R. Gregor, M. Rivera, A. Renault, and L. Comparatore, "Efficiency analysis of a modular H-bridge based on SiC-MOSFET," *Int. J. Electron. Letters*, vol. PP, no. 99, pp. 1–1, Early access, 2018.

[2] J.-H. Park and K.-B. Lee, "A two-stage bidirectional DC/DC converter with SiC-MOSFET for vehicle to grid (V2G) application," in *IEEE Proc. Energy Conversion, (CENCON2017)*, pp. 288–293.

[3] N. Hildebrandt, M. Petkovic, and D. Dujic, "Evaluation of 1.7 kv SiC-MOSFETs for a regenerative cascaded h-bridge multilevel converter cell," in *Proc. on Industrial Electronics, (ICIT2018)*, no. CONF.

[4] S. Toledo, E. Maqueda, M. Rivera, R. Gregor, D. Caballero, F. Gavilán, and J. Rodas, "Experimental assessment of igbt and SiC-MOSFET based technologies for matrix converter using predictive current control," in *IEEE Proc. Electrical, Electronics Engineering, Information and Communication Technologies (CHILECON2017)*, pp. 1–6.

[5] A. Renault, M. Rivera, L. Comparatore, J. Pacher, J. Rodas, and R. Gregor, "Model predictive current control with neutral current elimination for H-bridge two-level active power filters," in *IEEE Proc. (ETCM2016)*, pp. 1–5.

[6] O. González, J. Rodas, R. Gregor, M. Ayala, and M. Rivera, "Speed sensorless predictive current control of a five-phase induction machine," in *IEEE Proc. Industrial Electronics and Applications, (ICIEA2017)*, pp. 343–348.

[7] E. Maqueda, S. Toledo, D. Caballero, F. Gavilan, J. Rodas, M. Rivera, and P. Wheeler, "An experimental implementation of predictive control in direct matrix converter based on SiC-MOSFET bidirectional switches," in *IEEE Proc. (SPEEC2017)*, pp. 1–6.

[8] Z. Song, W. Chen, and C. Xia, "Predictive direct power control for three-phase grid connected converters without sector information and voltage vector selection," *IEEE Trans. on Power Electronics*, vol. 29, no. 10, pp. 5518–5531, 2014.

[9] C. Wang, Z. Du, Y. Ni, C. Li, and G. Zhang, "Coordinated predictive control for wind farm with bess considering power dispatching and equipment ageing," *IET Trans. IET Generation, Transmission & Distribution*, 2018.

[10] O. Romero, A. Olloqui, M. Macias, F. Martell, O. Micheloud, J. Elizondo, and M. Rivera, "Finite states-modulated model predictive control of a quasi-z-source inverter with lcl filter," in *IEEE Proc. Power Electronics, (SPEC2017)*, 2017, pp. 1–6.

[11] V. Gali, N. Gupta, and R. Gupta, "Mitigation of power quality problems using shunt active power filters: A comprehensive review," in *IEEE Proc. Industrial Electronics and Applications, (ICIEA2017)*, pp. 1100–1105.

[12] F. Li, F. He, Z. Ye, F. Tyrone, X. Wang, and X. Zhang, "A simplified pwm strategy for three-level converters on three-phase four-wire active power filter," *IEEE Trans. on Power Electronics*, vol. 33, no. 5, pp. 4396–4406, 2018.

[13] F. Sebaaly, H. Vahedi, H. Kanaan, and K. Al-Haddad, "Novel current controller based on mpc with fixed switching frequency operation for a grid-tied inverter," *IEEE Trans. on Industrial Electronics*, vol. 65, no. 8, pp. 6198–6205, 2018.

[14] A. Renault, M. Rivera, J. Rodas, L. Comparatore, J. Pacher, and R. Gregor, "Modulated model predictive current control for h-bridge two-level single phase active power filters statcom," in *IEEE Proc. Industrial Electronics and Applications, (ICIEA2017)*, pp. 355–359.

[15] L. Tarisciotti, A. Formentini, A. Gaeta, M. Degano, P. Zanchetta, R. Rabbeni, and M. Pucci, "Model predictive control for shunt active filters with fixed switching frequency," *IEEE Trans. on Industry Applications*, vol. 53, no. 1, pp. 296–304, 2017.

[16] Z. Yang, J. Sun, S. Li, M. Huang, X. Zha, and Y. Tang, "An adaptive carrier frequency optimization method for harmonic energy unbalance minimization in a cascaded h-bridge-based active power filter," *IEEE Trans. on Power Electronics*, vol. 33, no. 2, pp. 1024–1037, 2018.

[17] A. Mortezaei, M. Simões, T. Busarello, F. Marafão, and A. Al-Durra, "Grid-connected symmetrical cascaded multilevel converter for power quality improvement," *IEEE Trans. on Industry Applications*, vol. 54, no. 3, pp. 2792–2805, 2018.

[18] R. Gregor, A. Renault, L. Comparatore, J. Pacher, J. Rodas, D. Gregor, J. Munoz, and M. Rivera, "Finite-states model predictive control with increased prediction horizon for a 7-level cascade h-bridge multilevel statcom," in *Proc. (WMSCI2016)*, pp. 1–6.

[19] L. Comparatore, J. Rodas, M. Rivera, R. Gregor, J. Pacher, A. Renault, J. Muñoz, and P. Sanjeevikumar, "Model based predictive control with a fixed switching frequency applied to a single-phase cascade h-bridge multilevel statcom," in *IEEE Proc. Industrial Electronics and Applications (ICIEA2017)*, pp. 368–373.

[20] S. Ferreira, R. Gonzatti, R. Pereira, C. da Silva, L. da Silva, and G. Lambert, "Finite control set model predictive control for dynamic reactive power compensation with hybrid active power filters," *IEEE Trans. on Industrial Electronics*, vol. 65, no. 3, pp. 2608–2617, 2018.

[21] P. Falkowski and A. Sikorski, "Finite control set model predictive control for grid-connected ac–dc converters with lcl filter," *IEEE Trans. on Industrial Electronics*, vol. 65, no. 4, pp. 2844–2852, 2018.

[22] L. Comparatore, R. Gregor, J. Rodas, J. Pacher, A. Renault, and M. Rivera, "Model based predictive current control for a three-phase cascade h-bridge multilevel statcom operating at fixed switching frequency," in *IEEE Proc. Power Electronics for Distributed Generation Systems, (PEDG2017)*, pp. 1–6.

[23] R. Gregor, L. Comparatore, A. Renault, J. Rodas, J. Pacher, S. Toledo, and M. Rivera, "A novel predictive-fixed switching frequency technique for a cascade h-bridge multilevel statcom," in *IEEE Proc. Industrial Electronics Society, (IECON2016)*, pp. 3672–3677.